Appl. Phys. B 87, 685–691 (2007)
DOI: 10.1007/s00340-007-2649-z

Applied Physics B
Lasers and Optics

J. WANG
K.Y. WONG✉

Polarization characteristics of a light-emitting polymer microring laser

Department of Physics, The Chinese University of Hong Kong, Shatin, N.T., Hong Kong, P.R. China

Received: 27 September 2006/Revised version: 3 March 2007
Published online: 10 May 2007 • © Springer-Verlag 2007

ABSTRACT Microring cavities were fabricated by depositing poly(2-methoxy-5-(2′-ethylhexyloxy)-1,4-phenylene vinylene) (MEH-PPV) on glass fibers by a dip-coating method. Laser emissions in whispering gallery modes were observed by pumping with a frequency-doubled Nd:YAG laser. The threshold energy of the MEH-PPV microring laser was as low as 10 nJ per pulse (1.5 μJ/mm^2). The polarization characteristics of the microring lasers were studied and a polarization model was developed to explain the observed phenomena.

PACS 42.55.Sa; 42.70.Jk

1 Introduction

The rapid development of conjugated polymers as a new class of laser materials injects new opportunities into the research and design of laser devices [1]. The advantages of these materials include the availability of a large variety of synthetic procedures to tailor-make designed structures; low-cost fabrication processes, such as dip coating and spin coating to prepare thin-film waveguides; and the possibility to be electrically pumped. As an alternative to the conventional resonant cavity in a thin film waveguide structure, microcavities offer the advantage of being compact in size. Most types of microcavities, such as vertical microcavities [2], microdisks [3], and photonic crystals [4], are usually fabricated by rather complicated techniques. In contrast, the microring cavity has attracted much attention due to its simplified fabrication process. Microring lasers typically show low threshold energy, narrow line width lasing output, and high cavity quality factor. Microring lasing actions have been demonstrated in light-emitting polymers [5–11] and dye-doped polymers [3, 12–14].

Poly(2-methoxy-5-(2′-ethylhexyloxy)-1,4-phenylene vinylene) (MEH-PPV) is one of the best known light-emitting polymers. A number of applications based on MEH-PPV have been found in light-emitting diodes [15], photovoltaic cells [16], and laser devices [17, 18]. In this paper we demonstrate microring lasing actions from MEH-PPV thin films and investigate, both experimentally and theoretically, their polarization characteristics. By using a transverse pumping configuration, the polarization of the microring lasing output dramatically varied with the polarization of the pump light. Transverse electric (TE) mode lasing was observed when the microring laser was pumped by s-polarized, p-polarized, 45° linearly polarized, or circularly polarized light. No obvious transverse magnetic (TM) mode lasing was observed in all cases. A strong TE mode lasing emission was observed for s-polarized pumping, while, for p-polarized pumping, the quality of the TE mode lasing became poor and the output intensity seriously decreased. A near-threshold model was developed to explain the polarization phenomena of the microring laser. From the model, we found that the orientational distribution of the molecular dipole moments has significant contributions to the polarization characteristics of the microring lasers.

✉ Fax: +852-2603-5204, E-mail: kywong@phy.cuhk.edu.hk

2 Experiments

The microring cavity was fabricated by one-step coating the polymer solution upon a single-mode fiber. The MEH-PPV was used as received and dissolved in chlorobenzene in the dark and a nitrogen gas environment at room temperature. The MEH-PPV can normally be dissolved completely after stirring for 12 h. The final concentration varied from 5 g/l to 20 g/l, which, in combination with the speed of the dip coating, determine the thickness of the films. In order to vary the diameter of the fibers, and hence the cavity volume, the fibers were etched at room temperature in low-concentration hydrofluoric acid. Depending on the etching time, fibers with diameters varying from the original size of 125 μm to 45 μm were obtained. The coating process was completed by dipping the etched fiber into a polymer solution using a home-made dip coater. After the subsequent quick evaporation, a uniform active layer was formed around the cylindrical core. The thickness of the polymer layer was estimated to be > 1 μm with the dip speed of 0.75 mm/s in the 20 g/l solution.

A schematic diagram of the experimental setup for studying the microring laser is illustrated in Fig. 1. A transverse pumping configuration was adopted. The frequency-doubled output from a nanosecond Nd:YAG laser that served as the pumping source was s-polarized. Polarizing optics and wave plates were inserted in the optical path wherever necessary to

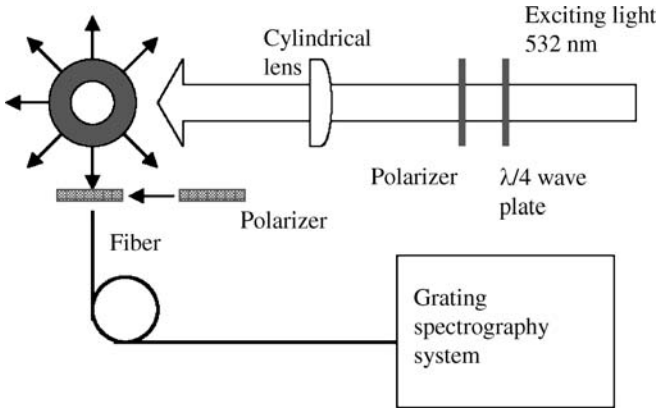

FIGURE 1 Experimental setup for the study of the microring laser

control the polarization property of the pump beam. The pump beam was focused onto the fiber by a cylindrical lens. The lasing output emerges from every point on the circumference of the microring, instead of in the form of a single beam of light from an ordinary Fabry–Pérot laser. This unconventional output may find specific applications in the future. A 0.3 m spectrograph/array detector system was employed for spectral measurements of the laser output. The spectral resolution of the detection system was 0.5 nm, which is adequate to resolve the multi-mode emission lines of the microring laser.

Multi-mode lasing from an MEH-PPV microring cavity with an outer diameter D of 50 μm was observed at a pump energy of 100 nJ per pulse. Accounting for reflection, transmission, and scattering losses of the pump laser, the actual energy delivered to the film was about 10 nJ per pulse (1.5 $\mu J/mm^2$). Figure 2a shows the emission spectra of the MEH-PPV microring laser at different excitation energies. When the pump energy reached the threshold, multi-wavelength lasing at fixed wavelengths appeared on top of the amplified spontaneous emission (ASE) background. The lasing intensity increased significantly as the pump energy increased, while the wavelength of each mode remained constant. Figure 2b shows the emission intensity as a function of the exciting energy. The emission intensities were obtained by integrating over all the lasing peaks. By increasing the pump energy, the output intensity increased linearly. The threshold energy was determined to be about 10 nJ per pulse. Saturation of the emission was observed when the pump energy exceeded 90 nJ per pulse. Saturation in the high pump energy region was attributed to gain saturation and degradation of the sample [6].

Figure 3 shows a typical spectrum of an MEH-PPV microring laser with an approximate diameter of 50 μm. The average mode separation $\Delta\lambda$ was measured to be 1.48 nm. $\Delta\lambda$ can be theoretically estimated by [7]

$$\Delta\lambda = \frac{\lambda^2}{2\pi R_0 \eta}\,, \tag{1}$$

where R_0 is the outer radius of the ring and η is the effective refractive index of a waveguided mode. By setting the effective refractive index to be 1.63, we observed good agreement between experiment and theory, as shown in the inset of Fig. 3. The azimuthal mode number M was determined by [3]

$$2\pi R_0 \eta = M\lambda_M\,, \tag{2}$$

and the radial mode number N was kept at 1 [13]. As indicated in Fig. 3, M ranged from 409 to 420. When a microring of diameter 80 μm was used instead, the lasing emission with an average mode separation $\Delta\lambda$ of 1.00 nm was observed. As shown in the inset of Fig. 3, good agreement between theory and experiment was also obtained. The corresponding azimuthal mode number ranged from 608 to 622.

Polarization characteristics of the microring laser were studied by changing the state of polarization of the pump light. The microring lasing emission was analyzed by a polarizer that was placed in front of the fiber in conjunction with the

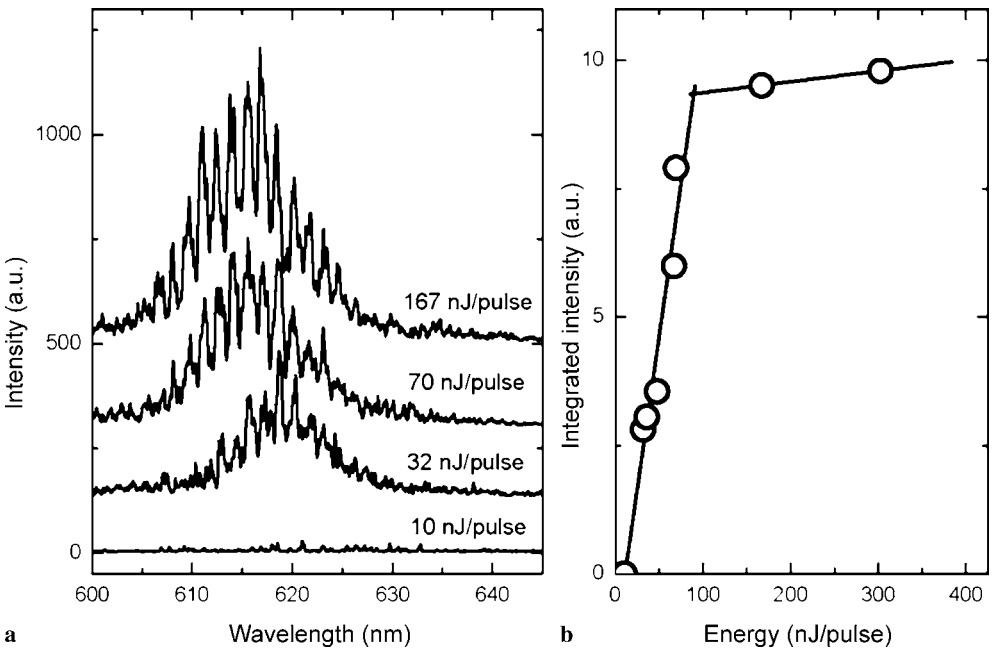

FIGURE 2 (**a**) Emission spectra of a 50-μm-diameter MEH-PPV microring laser by transverse pumping at four different excitation energies. (**b**) Emission intensity as a function of excitation energy

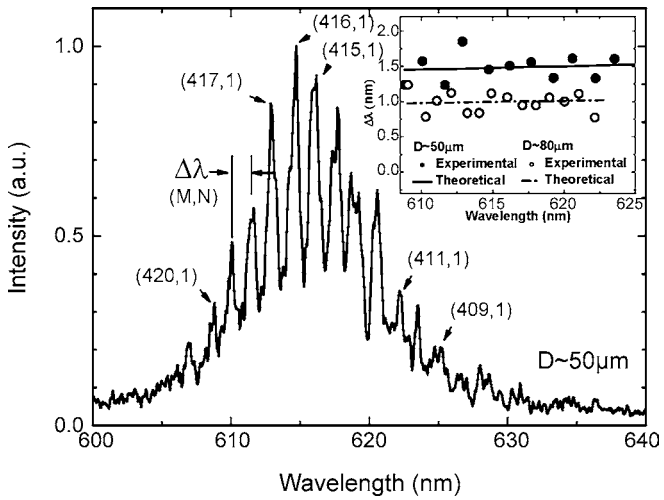

FIGURE 3 A typical output spectrum for a 50-μm-diameter MEH-PPV microring laser. *Inset*: mode separations Δλ for microring lasers with two different diameters

detector, as shown in Fig. 1. TE and TM lasing modes can be separately detected by rotating the transmission axis of the analyzer to a parallel or perpendicular orientation with respect to the fiber axis of the microring. Figure 4 shows the output spectra for a 50-μm-diameter MEH-PPV microring laser by s-polarized pumping, p-polarized pumping, 45° linearly polarized pumping, and circularly polarized pumping, respectively. The lasing output dramatically changed with the pump polarization. We use the polarization ratio P, defined by $P = I_{TE}/I_{TM}$, as a measurement of the polarization state of the microring lasing output. For s-polarized pumping, strong TE mode lasing emission was observed and $P_s \cong 140$. For p-polarized pumping, the quality of the TE mode lasing became poor and the output intensity seriously decreased. While the TM mode lasing shows no significant decrease, the polarization ratio P_p reduced to approximately 9. For the other two pumping schemes, the values of P lie between P_s and P_p. These polarization phenomena are consistent with those reported previously, but no quantitative explanation was given [5]. We note that although the pump energy is close to the saturation value (see also Fig. 2b), the TM mode lasing was observed to be very weak in all cases.

The suppression of TM modes of a microring laser is in contrast to the polarization phenomena of a planar thin film waveguide laser that we studied previously [19]. For a planar waveguide laser, significant TM mode lasing can be generated by p-polarized and circularly polarized pumping. It was suspected that the suppression of the TM mode could be a result of the preferential orientation of the polymer chains in

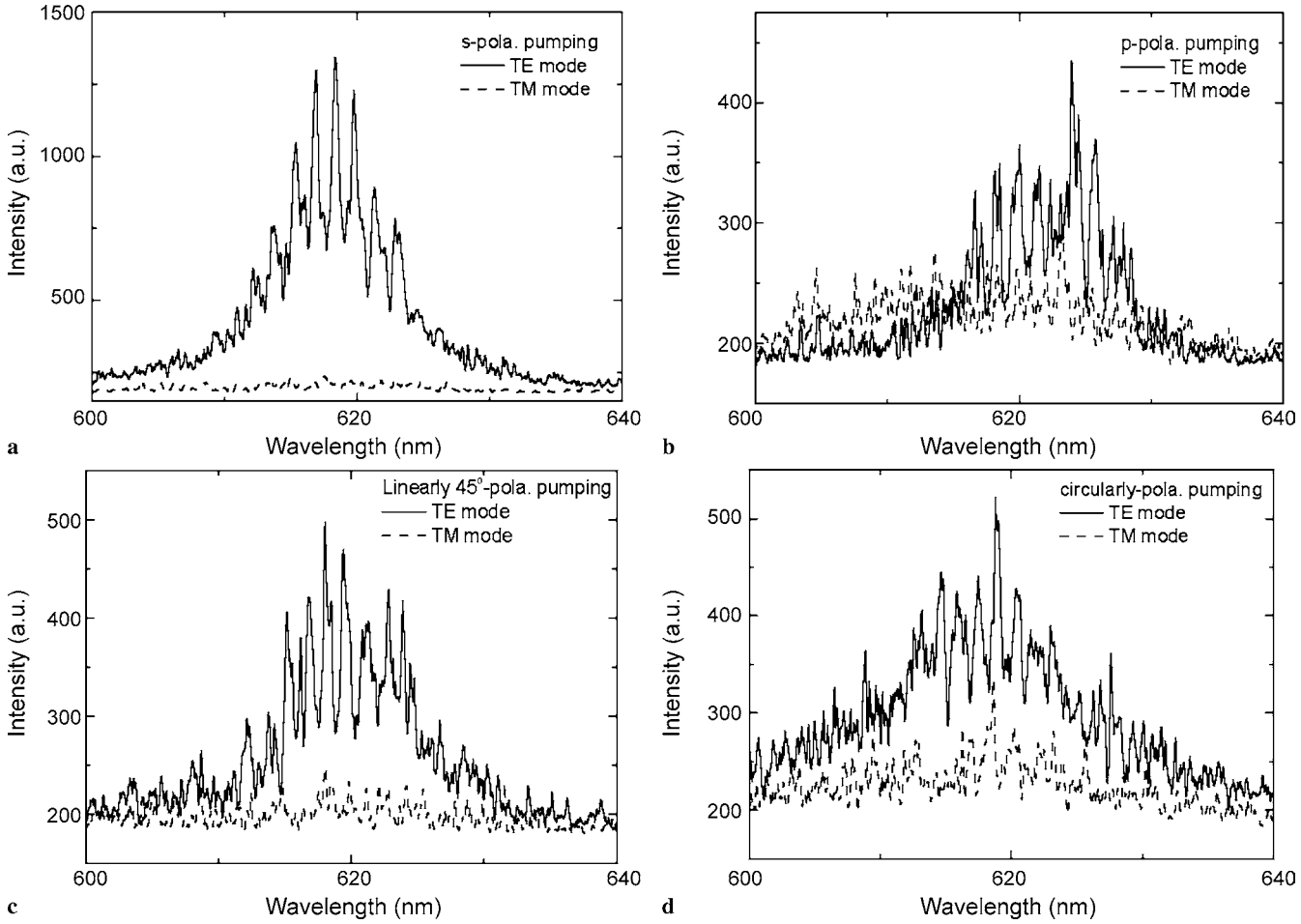

FIGURE 4 Output spectra for a 50-μm-diameter MEH-PPV microring laser with (**a**) s-polarized pumping, (**b**) p-polarized pumping, (**c**) 45° linearly polarized pumping, and (**d**) circularly polarized pumping

the plane of the substrate [20]; however, no quantitative investigation was performed. In Sect. 3, we will present a near-threshold polarization model of microring lasers for a transverse pumping configuration. In the model, the orientational distribution of the dipole moment of the excitons in the MEH-PPV film is assumed to be either

1. a three-dimensional isotropic distribution (3-D) or
2. a two-dimensional random distribution in the plane of the fiber substrate (2-D).

The small-signal gain coefficients for s-polarized, p-polarized, and 45°-polarized pumping schemes will be calculated for the two orientational distribution models and compared with the experiment.

3 Theory

For the calculation of the gain coefficients, we shall adapt the semi-classical amplifier theory developed by Reyzer and Casperson [21, 22] for a dye laser. In this approach, the frozen-dipole approximation was used such that the reorientation of the lasing dye molecules as a result of rotational diffusion was assumed to be negligible. Since we are dealing with a solid state polymer film, the physical reorientation of the polymer chain is clearly not possible. On the other hand, it is generally known that through certain internal energy coupling processes such as Förster transfer, energy from an excited exciton localized in a conjugated segment can be transferred to another exciton of lower energy in another segment. This energy transfer, which results in the red shift of the luminescence peak, was found to occur in the first few picoseconds after an optical excitation [23]. This stochastic energy transfer process will cause a randomization of the orientations of the emitting dipoles and it may appear that the frozen-dipole approximation is not applicable. However, it was found that in a conjugated polymer, the onset of the stimulated emission (SE) line narrowing is concomitant with a blue shift of the emission peak [24]. The blue shifting of the SE peak compared to the non-SE peak indicates that the SE spectrum draws the gain from excited species that are without internal relaxation. It was thus concluded that stimulated emission occurs on a time scale faster than interchain energy migration [24]. Since the orientations of the emitting dipoles that are responsible for lasing can be regarded to be largely undisturbed before internal relaxations cause the randomization, we therefore assume the frozen-dipole approximation to be valid and employ the theory developed by Reyzer and Casperson [21, 22] to calculate the gain coefficients.

The gain coefficients for the two orthogonal polarizations along the propagation direction are defined by [21]

$$\alpha_x = \sigma_\mathrm{s} \int_\Omega n(\theta,\varphi) D_\mathrm{s} \cos^2\theta \,\mathrm{d}\Omega \,, \tag{3a}$$

$$\alpha_y = \sigma_\mathrm{s} \int_\Omega n(\theta,\varphi) D_\mathrm{s} \sin^2\theta \cos^2\varphi \,\mathrm{d}\Omega \,, \tag{3b}$$

where σ_s is the stimulated emission cross section, $n(\theta,\varphi)\,\mathrm{d}\Omega$ is the molecular number density in the solid angle $\mathrm{d}\Omega$ along the (θ,φ) direction, and D_s is the population difference between the two energy states where the stimulated transition takes place. Assuming no pump saturation, D_s is linearly dependent on the pump intensity, and is given by

$$D_\mathrm{s} = \frac{\tau\sigma_\mathrm{p}}{h\nu_\mathrm{p}} \frac{\varepsilon c}{2n_0} \left|\boldsymbol{E}_\mathrm{p}\boldsymbol{\mu}\right|^2 \,, \tag{4}$$

where τ is the fluorescence decay time, σ_p is the absorption cross section, $h\nu_\mathrm{p}$ is the photon energy of the pump light, $\boldsymbol{E}_\mathrm{p}$ is the complex amplitude of the pump field, and the term $\varepsilon c/2n_0$ relates the electric field with the light intensity. The orientation of the dipole moments μ is represented by the Euler angles (θ,φ), which is expressed in Cartesian coordinates by

$$\boldsymbol{\mu} = (\hat{x}\cos\theta + \hat{y}\sin\theta\cos\varphi + \hat{z}\sin\theta\sin\varphi)\,|\boldsymbol{\mu}| \,. \tag{5}$$

For an isotropic distribution of the dipole moment orientations, we have

$$n(\theta,\varphi) = N/4\pi \,, \tag{6}$$

where N is the number density of the gain medium. By assuming that each singlet exciton extends over 10 repeat units of MEH-PPV [25], we estimate N to be approximately $2\times10^{20}\,\mathrm{cm}^{-3}$. Substituting (4) and (6) into (3), we can express the gain coefficients for the TE and TM modes by

$$g_\mathrm{TE} = C_0 \int_\Omega \left|\boldsymbol{E}_\mathrm{p}\boldsymbol{\mu}\right|^2 \cos^2\theta \,\mathrm{d}\Omega \,, \tag{7a}$$

$$g_\mathrm{TM} = C_0 \int_\Omega \left|\boldsymbol{E}_\mathrm{p}\boldsymbol{\mu}\right|^2 \sin^2\theta\cos^2\varphi \,\mathrm{d}\Omega \,, \tag{7b}$$

where

$$C_0 = \frac{N}{4\pi}\frac{\tau\sigma_\mathrm{s}\sigma_\mathrm{p}}{h\nu_\mathrm{p}}\frac{\varepsilon c}{2n_0}.$$

For s-polarized pumping, the exciting field $\boldsymbol{E}_\mathrm{p}$ can be written as

$$\boldsymbol{E}_\mathrm{p} = E_\mathrm{p} t_\mathrm{s}(\psi)\hat{e}_x \,, \tag{8}$$

where $t_\mathrm{s}(\psi)$ is the transmissivity of the s-polarized wave that is given by the Fresnel formula

$$t_\mathrm{s}(\psi) = \frac{2\cos\psi}{\cos\psi + \sqrt{n^2 - \sin^2\psi}} \,, \tag{9}$$

where n is the refractive index of the MEH-PPV film and ψ is the azimuthal angle as shown in Fig. 5. Substituting (8) into (7), we obtain the azimuthal-angle-dependent gain coefficients of the form

$$g_\mathrm{TE}(\psi) = C_1 t_\mathrm{s}(\psi)^2 \,, \tag{10a}$$

$$g_\mathrm{TM}(\psi) = \frac{1}{3} C_1 t_\mathrm{s}(\psi)^2 \,, \tag{10b}$$

where

$$C_1 = \frac{4\pi}{5} C_0 E_\mathrm{p}^2 = \frac{N\tau\sigma_\mathrm{s}\sigma_\mathrm{p}}{5h\nu_\mathrm{p}} I_\mathrm{p} \,. \tag{11}$$

At near-threshold conditions, the exciting intensity $I_\mathrm{p} = 1.5\times10^5\,\mathrm{W\,cm}^{-2}$ (100 nJ per pulse), the average number

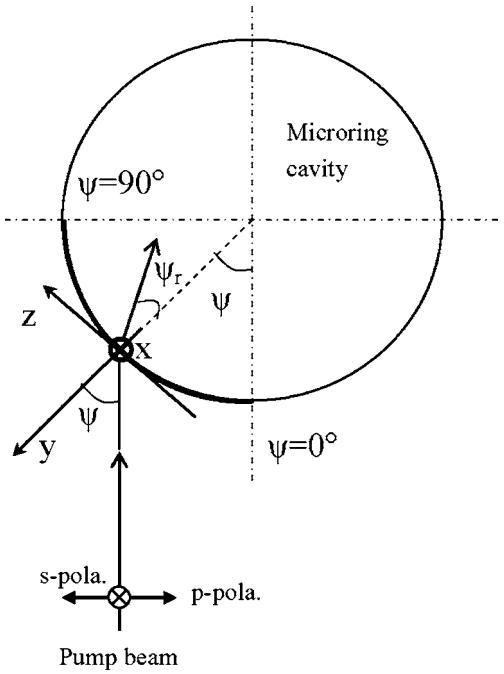

FIGURE 5 A schematic representation of the pumping geometry

density $N = 2 \times 10^{20}\,\mathrm{cm}^{-3}$, the absorption and stimulated emission cross sections $\sigma_\mathrm{p} \approx \sigma_\mathrm{s} \approx 1.2 \times 10^{-17}\,\mathrm{cm}^2$ [26], and the fluorescence decay time $\tau = 260$ ps [27]. Thus, a value of the threshold gain factor C_1 of $6 \times 10^{-2}\,\mathrm{mm}^{-1}$ is estimated for the TE mode by s-polarized pumping. The total gain can be obtained by integrating (10). Due to the symmetrical geometry, we only need to consider the first quadrant $0° \le \psi \le 90°$ as shown in Fig. 5. Then, the average gain coefficients in the first quadrant can be written as

$$G_\mathrm{TE} = \frac{2}{\pi} C_1 \int_0^{\pi/2} t_\mathrm{s}(\psi)^2 \,\mathrm{d}\psi \,, \tag{12a}$$

$$G_\mathrm{TM} = \frac{2}{3\pi} C_1 \int_0^{\pi/2} t_\mathrm{s}(\psi)^2 \,\mathrm{d}\psi \,. \tag{12b}$$

The p-polarized exciting field has the form

$$\boldsymbol{E}_\mathrm{p} = E_\mathrm{p} t_\mathrm{p}(\psi) \sin\psi_\mathrm{r} \hat{e}_y + E_\mathrm{p} t_\mathrm{p}(\psi) \cos\psi_\mathrm{r} \hat{e}_z \,, \tag{13}$$

where the refraction angle ψ_r is related to ψ by $\psi_\mathrm{r} = \arcsin(\sin\psi/n)$. $E_\mathrm{p} t_\mathrm{p}(\psi) \sin\psi_\mathrm{r}$ and $E_\mathrm{p} t_\mathrm{p}(\psi) \cos\psi_\mathrm{r}$ are the contributions of E_p in the y and z directions, respectively. $t_\mathrm{p}(\psi)$ is the transmissivity of the p-polarized wave, which is given by

$$t_\mathrm{p}(\psi) = \frac{2n\cos\psi}{n^2\cos\psi + \sqrt{n^2 - \sin^2\psi}} \,. \tag{14}$$

The angle-dependent gain coefficients are obtained by substituting (13) into (7) to give

$$g_\mathrm{TE}(\psi) = \frac{1}{3} C_1 t_\mathrm{p}(\psi)^2 \,, \tag{15a}$$

$$g_\mathrm{TM}(\psi) = C_1 t_\mathrm{p}(\psi)^2 \left(\sin^2\psi_\mathrm{r} + \frac{1}{3}\cos^2\psi_\mathrm{r} \right) \,. \tag{15b}$$

The corresponding average gain coefficients are of the form

$$G_\mathrm{TE} = \frac{2}{3\pi} C_1 \int_0^{\pi/2} t_\mathrm{p}(\psi)^2 \,\mathrm{d}\psi \,, \tag{16a}$$

$$G_\mathrm{TM} = \frac{2}{\pi} C_1 \int_0^{\pi/2} \left(\sin^2\psi_\mathrm{r} + \frac{1}{3}\cos^2\psi_\mathrm{r} \right) t_\mathrm{p}(\psi)^2 \,\mathrm{d}\psi \,. \tag{16b}$$

The electric field for a 45°-polarized exciting field is given by

$$\boldsymbol{E}_\mathrm{p} = \frac{\sqrt{2}}{2} E_\mathrm{p} t_\mathrm{s}(\psi) \hat{e}_x + \frac{\sqrt{2}}{2} E_\mathrm{p} t_\mathrm{p}(\psi) \sin\psi_\mathrm{r} \hat{e}_y + \frac{\sqrt{2}}{2} E_\mathrm{p} t_\mathrm{p}(\psi) \cos\psi_\mathrm{r} \hat{e}_z \,. \tag{17}$$

Similarly, the expressions for the angle-dependent gain coefficients and the average gain are respectively given by

$$g_\mathrm{TE}(\psi) = \frac{1}{2} C_1 t_\mathrm{s}(\psi)^2 + \frac{1}{6} C_1 t_\mathrm{p}(\psi)^2 \,, \tag{18a}$$

$$g_\mathrm{TM}(\psi) = \frac{1}{6} C_1 t_\mathrm{s}(\psi)^2 + \frac{1}{2} C_1 t_\mathrm{p}(\psi)^2 \left(\sin^2\psi_\mathrm{r} + \frac{1}{3}\cos^2\psi_\mathrm{r} \right) \,, \tag{18b}$$

and

$$G_\mathrm{TE} = \frac{1}{\pi} C_1 \int_0^{\pi/2} \left[t_\mathrm{s}(\psi)^2 + \frac{1}{3} t_\mathrm{p}(\psi)^2 \right] \mathrm{d}\psi \,, \tag{19a}$$

$$G_\mathrm{TM} = \frac{1}{\pi} C_1 \int_0^{\pi/2} \left[\frac{1}{3} t_\mathrm{s}(\psi)^2 + (\sin^2\psi_\mathrm{r} + \frac{1}{3}\cos^2\psi_\mathrm{r}) t_\mathrm{p}(\psi)^2 \right] \mathrm{d}\psi \,. \tag{19b}$$

In addition, a circularly polarized exciting field is of the form

$$\boldsymbol{E}_\mathrm{p} = \mathrm{i}\frac{\sqrt{2}}{2} E_\mathrm{p} t_\mathrm{s}(\psi) \hat{e}_x + \frac{\sqrt{2}}{2} E_\mathrm{p} t_\mathrm{p}(\psi) \sin\psi_\mathrm{r} \hat{e}_y + \frac{\sqrt{2}}{2} E_\mathrm{p} t_\mathrm{p}(\psi) \cos\psi_\mathrm{r} \hat{e}_z \,. \tag{20}$$

The expressions for the angle-dependent gain coefficients and the average gain obtained are the same as those for a 45°-polarized pumping scheme.

Alternatively, assuming that the polymer chains lie only in the plane of the substrate, the orientation of the dipole moments $\boldsymbol{\mu}$ can be written in the form

$$\boldsymbol{\mu} = (\hat{x}\cos\theta + \hat{z}\sin\theta)\,|\boldsymbol{\mu}| \tag{21}$$

and

$$n(\theta) = N/2\pi \,. \tag{22}$$

By substituting (8), (13), and (17) into (7) along with (21) and (22), we can obtain the angle-dependent gain coefficients for s-polarized, p-polarized, and 45°-polarized pumping schemes, respectively, in the forms

$$g_{\mathrm{TE}}^{\mathrm{s}}(\psi) = \frac{15}{8} C_1 t_{\mathrm{s}}(\psi)^2 \,, \tag{23a}$$

$$g_{\mathrm{TE}}^{\mathrm{p}}(\psi) = \frac{5}{8} C_1 t_{\mathrm{p}}(\psi)^2 \cos^2 \psi_{\mathrm{r}} \,, \tag{23b}$$

$$g_{\mathrm{TE}}^{\mathrm{l}}(\psi) = \frac{15}{16} C_1 t_{\mathrm{s}}(\psi)^2 + \frac{5}{16} C_1 t_{\mathrm{p}}(\psi)^2 \cos^2 \psi_{\mathrm{r}} \,. \tag{23c}$$

Correspondingly, their average gains are given by

$$G_{\mathrm{TE}}^{\mathrm{s}} = \frac{15}{4\pi} C_1 \int_0^{\pi/2} t_{\mathrm{s}}(\psi)^2 \,\mathrm{d}\psi \,, \tag{24a}$$

$$G_{\mathrm{TE}}^{\mathrm{p}} = \frac{5}{4\pi} C_1 \int_0^{\pi/2} t_{\mathrm{p}}(\psi)^2 \cos^2 \psi_{\mathrm{r}} \,\mathrm{d}\psi \,, \tag{24b}$$

$$G_{\mathrm{TE}}^{\mathrm{l}} = \frac{5}{8\pi} C_1 \int_0^{\pi/2} \left[3 t_{\mathrm{s}}(\psi)^2 + t_{\mathrm{p}}(\psi)^2 \cos^2 \psi_{\mathrm{r}} \right] \mathrm{d}\psi \,. \tag{24c}$$

Since the dipoles are oriented only in the x–z plane, they have no component along the y direction. This results in the vanishing of the gain for TM mode lasing in all cases.

Distribution of dipoles	3-D		2-D	
Average gain ($\times 10^{-3}$, mm^{-1})	G_{TE}	G_{TM}	G_{TE}	G_{TM}
s-polarized	16.66	5.55	31.24	0
p-polarized	6.42	7.62	10.90	0
45°-polarized	11.54	6.59	21.07	0

TABLE 1 Summary of the average gains of the MEH-PPV microring cavity for different pumping schemes

Figure 6 presents the gain as a function of the azimuthal angle ψ for an MEH-PPV microring cavity. The refractive index of MEH-PPV is 1.94, and the gain factor C_1 is set to 6×10^{-2} mm^{-1}. Figure 6a–c illustrate the gain variations for the case of a 3-D isotropic distribution of the dipole moments. Figure 6d illustrates the situation for a 2-D distribution. The average gains, which are obtained by numerical integration, are summarized in Table 1. For the TE mode in a 3-D distribution, the average gain is larger for s-polarized pumping and is smaller for p-polarized pumping. The situation is the same for the TE mode in a 2-D distribution. In contrast, the gains of the TM mode essentially remained constant for different pumping schemes in the 3-D distribution case, while the gains of the TM mode become zero for the 2-D case. From the ex-

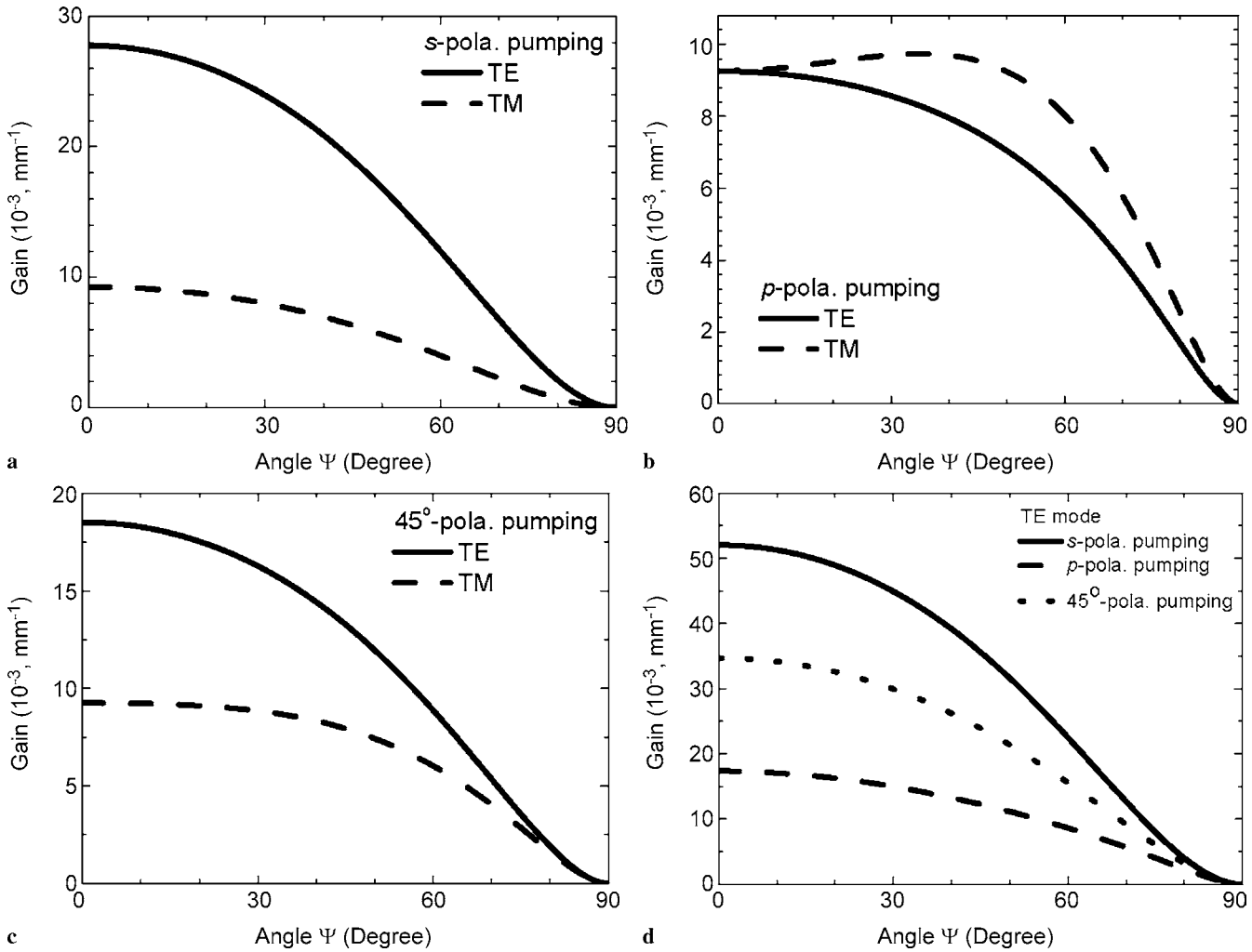

FIGURE 6 Angle-dependent gain coefficients of the MEH-PPV microring cavity for different pump beam polarizations. In (**a**)–(**c**) a 3-D isotropic distribution of the dipole moment is assumed; in (**d**) a 2-D random distribution of the dipole moment is assumed

perimental results in Fig. 4, we can see that the variation of the TE mode lasing intensity with the pumping polarization is consistent with the gain variation predicted by our theoretical modeling. On the other hand, the suppression of TM mode lasing can only be explained by the theoretical modeling assuming a 2-D distribution. That is to say, most of the MEH-PPV polymer chains lie in the plane of the fiber substrate. This quasi-2-D distribution of the dipole moments leads to the observed polarization phenomena.

4 Conclusion

Microring lasers based on MEH-PPV were demonstrated. For a 50-μm-diameter microring laser, the pumping threshold was 10 nJ per pulse. The lasing modes were identified. The polarization characteristics were studied and a near-threshold model was developed to explain the polarization phenomena. A 2-D distribution of the dipole moments is required to account for the polarization characteristics of the microring lasers. The model could be applied to the transverse pumped laser cavities with different geometries such as microspheres and microdisks.

ACKNOWLEDGEMENTS One of us (J.W.) would like to thank Ms. F. Chen for her helpful discussions regarding this work.

REFERENCES

1 M.D. McGehee, A.J. Heeger, Adv. Mater. **12**, 1655 (2000)
2 N. Tessler, G.J. Denton, R.H. Friend, Nature **382**, 695 (1996)
3 M. Kuwata-Gonokami, R.H. Jordan, A. Dodabalapur, H.E. Katz, M.L. Schilling, R.E. Slusher, S. Ozawa, Opt. Lett. **20**, 2093 (1995)
4 M. Meier, A. Mekis, A. Dodabalapur, A. Timko, R.E. Slusher, J.D. Joannopoulos, O. Nalamasu, Appl. Phys. Lett. **74**, 7 (1999)
5 S.V. Frolov, M. Shkunov, Z.V. Vardeny, K. Yoshino, Phys. Rev. B **56**, R4363 (1997)
6 Y. Kawabe, C. Spiegelberg, A. Schulzgen, M.F. Nabor, B. Kippelen, E.A. Mash, P.M. Allemand, M. Kuwata-Gonokami, K. Takeda, N. Peyghambarian, Appl. Phys. Lett. **72**, 141 (1998)
7 S.V. Frolov, Z.V. Vardeny, K. Yoshino, Appl. Phys. Lett. **72**, 1802 (1998)
8 S.V. Frolov, A. Fujii, D. Chinn, M. Hirohata, R. Hidayat, M. Taraguchi, T. Masuda, K. Yoshino, Z.V. Vardeny, Adv. Mater. **10**, 869 (1998)
9 R. Österbacka, M. Wohlgenannt, M. Shkunov, D. Chinn, Z.V. Vardeny, J. Chem. Phys. **118**, 8905 (2003)
10 Y. Yashida, Y. Nishihara, A. Fujii, M. Ozaki, K. Yoshino, H.K. Kim, N.S. Baek, S.K. Choi, J. Appl. Phys. **95**, 4193 (2004)
11 Y. Yoshida, T. Nishimura, A. Fujii, M. Ozaki, K. Yoshino, Appl. Phys. Lett. **86**, 141 903 (2005)
12 G. Wirnsberger, G.D. Stucky, Chem. Mater. **12**, 2525 (2000)
13 T. Ben-Messaoud, S.X. Dou, E. Toussaere, A. Potter, D. Josse, G. Kranzelbinder, J. Zyss, Synth. Met. **127**, 159 (2002)
14 T. Kobayashi, M. Djiango, G. Jordan, M. Rüther, W.J. Blau, Y. Suzuki, T. Kaino, Appl. Phys. Lett. **88**, 181 119 (2006)
15 Y. Shi, J. Liu, Y. Yang, Macromol. Symp. **154**, 187 (2000)
16 J. Gao, G. Yu, A.J. Heeger, Adv. Mater. **10**, 692 (1998)
17 G.A. Turnbull, T.F. Krauss, W.L. Barnes, I.D.W. Samuel, Synth. Met. **121**, 1757 (2001)
18 A.M. Familia, A. Sarangan, T.R. Nelson, Opt. Express **13**, 3136 (2005)
19 C. Ye, L. Shi, J. Wang, D. Lo, X.L. Zhu, Appl. Phys. Lett. **83**, 4101 (2003)
20 M.D. McGehee, M.A. Diaz-Garcia, F. Hide, R. Gupta, E.K. Miller, D. Moses, A.J. Heeger, Appl. Phys. Lett. **72**, 1536 (1998)
21 K.C. Reyzer, L.W. Casperson, J. Appl. Phys. **51**, 6075 (1980)
22 K.C. Reyzer, L.W. Casperson, J. Appl. Phys. **51**, 6083 (1980)
23 G.R. Hayes, I.D.W. Samuel, R.T. Phillips, Phys. Rev. B **52**, R11 569 (1995)
24 M.A. Diaz-Garcia, F. Hide, B.J. Schwartz, M.R. Andersson, Q. Pei, A.J. Heeger, Synth. Met. **84**, 455 (1997)
25 D. Beljonne, Z. Shuai, R.H. Friend, J.L. Bredas, J. Chem. Phys. **102**, 2042 (1995)
26 L. De Boni, A.A. Andrade, D.S. Correa, D.T. Balogh, S.C. Zilio, L. Misoguti, C.R. Mendonca, J. Phys. Chem. B **108**, 5221 (2004)
27 G. Ma, L. Guo, J. Mi, Y. Liu, S. Qian, J. Liu, G. He, Y. Li, R. Wang, Physica B **305**, 147 (2001)